Friction and Adhesion Hysteresis of Fluorocarbon Surfactant Monolayer-Coated Surfaces Measured with the Surface Forces Apparatus

Shinji Yamada[†] **and Jacob Israelachvili***

Department of Chemical Engineering and Materials Department, University of California, Santa Barbara, California 93106

Received: September 3, 1997[⊗]

Friction and adhesion hysteresis experiments were carried out on fluorocarbon surfactant monolayer-coated surfaces using the surface forces apparatus. Measurements were made as a function of temperature, load, sliding velocity, and relaxation time, and the resulting properties are contrasted with those of hydrocarbon monolayers and also with bulk fluorocarbon surfaces (e.g., Teflon, PTFE). The dynamic adhesion measurements show that the adhesion hysteresis and friction of fluorocarbon monolayer-coated surfaces are related: large friction forces being associated with large adhesion hysteresis. The results also show that the overall tribological properties of fluorocarbon surfactants follow the same generic "friction phase diagram" behavior as do hydrocarbon surfactants. However, the friction phase diagram for fluorocarbon surfactant has at least two peaks—one well above and the other well below room temperature—indicating that two different molecular relaxation processes are involved in friction and adhesion energy dissipation. Apparently, chain interdigitation, which is the most important molecular relaxation mechanism in the friction and adhesion hysteresis of hydrocarbon materials, does not play a major role with fluorocarbon surfaces. Instead, the surface topography and its change at the molecular and submolecular levels during shear is the most important factor determining the friction of these surfaces, but only so long as the monolayers remain molecularly smooth or "undamaged". Reasons for the beneficial tribological properties of fluorocarbon surfaces are discussed.

Introduction

Reducing friction and wear is one of the most important requirements for improving the performance of moving components in many technological devices. Various kinds of lubricants have been developed for attaining low friction and wear, and many experimental and theoretical studies have recently been carried out on the rheology and tribology of ultrathin lubricating films of various organic molecules, especially hydrocarbon surfactants and liquids, using the surface forces apparatus technique.[1−6] On the other hand, fluorocarbon materials and surfaces are also widely used in certain technologies to prepare low-energy, low-friction surfaces. Many of these are "boundary lubricants", which are surfactants or polymers having certain molecular structures and functional groups for attaching the molecules, either chemically or physically, to the substrate surfaces.[7,8] For some kinds of lubricants, being chemically bound or otherwise strongly attached to the substrate surface is very important. For example, lubricants used for magnetic recording disks must form a thin strongly bound surface layer if they are to perform well as a lubricant, i.e., exhibit low friction and wear over long time periods. If the lubricant molecules are not strongly and uniformly adsorbed, but are movable, they easily spin off during high-speed rotation of the disks or their thickness distribution on the disk becomes very nonuniform—usually at the edge—during rotation.[9] These two factors act to decrease the efficiency and lifetime of disks. For these reasons, the friction behavior of fluorocarbon materials with functional groups is of major interest in the technological devices field.

In this study, we investigated the friction and adhesion properties of a fluorocarbon surfactant. The reason we chose a surfactant was as follows: some kinds of fluorocarbon surfactants are easy to deposit as monolayers of known coverage by the Langmuir−Blodgett deposition method. This allowed us to compare the tribological behavior of fluorocarbon monolayers, prepared and tested under different but well-controlled conditions, and also compare their behavior with analogous and similarly prepared hydrocarbon surfactant monolayers.

Materials and Methods

Surface Forces Apparatus. The surface forces apparatus (SFA) used in this study was a SFA3.[10] Generally, two cylindrical mica surfaces, each of a radius $R \approx 1$ cm, are positioned in a crossed cylinder configuration. The two surfaces are brought toward or away from each other using several mechanical stages of increasing sensitivity. An optical technique using multiple beam interference fringes (FECO) is used to "observe" and monitor the contact region of the two surfaces.[11] From the positions and shapes of the FECO fringes, one can measure the undeformed radius, R, of the surfaces and the distance between them, D, to within 1 Å. When two surfaces are pressed together under an external load, L, the surfaces usually flatten elastically as shown in Figure 1. The flattened contact radius, r, and area, $A = \pi r^2$, and the trapped film thickness, D, can also be directly measured with the FECO fringes.

Adhesion Hysteresis Measurements. Adhesion energies γ (see Figure 1) were determined from the contact area−load dependence, and the results were analyzed in terms of the Johnson−Kendall−Roberts (JKR) theory of contact mechanics.[12] The JKR equation is

[†] On leave from Kao Corporation, Japan.
[⊗] Abstract published in *Advance ACS Abstracts,* December 15, 1997.

S1089-5647(97)02875-7 CCC: $15.00 © 1998 American Chemical Society
Published on Web 01/01/1998

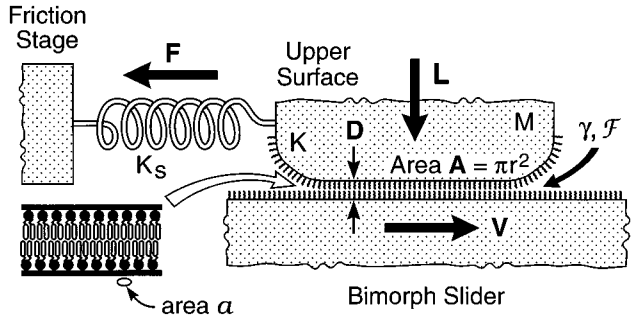

Figure 1. Schematic geometry of the contact region of the basic tribological system: two surfactant-coated mica surfaces in the surface forces apparatus. Typical values were true contact area, $A = \pi r^2 = 1-5 \times 10^{-9}$ m^2; externally applied normal load, $L = 0-150$ mN; sliding velocity, $V = 0.001-100$ μm/s. K_S is the elastic stiffness of the spring which couples the drive or translation stage to the upper mica surface; F is the measured friction force (which may be different from the instantaneous friction force $\mathcal{F}$ acting at the interface), a is the molecular area per surfactant molecule, γ is the surface energy, D is the film thickness, K is the (Hertzian) elastic modulus of the surfaces, and M is the mass of the upper surface.

$$r^3 = \frac{R}{K}[L + 6\pi R\gamma + \sqrt{12\pi R\gamma L + (6\pi R\gamma)^2}] \qquad (1)$$

where R is the undeformed radius of the sphere and K is the elastic modulus of the materials. From eq 1 one can obtain the loading (advancing) or unloading (receding) energies, γ_A and γ_R, depending on whether the load (or contact area) is being increased or decreased. Under ideal, thermodynamically reversible conditions, r^3-L curves should follow the same path on loading and unloading because $\gamma_A = \gamma_R$. Such results have indeed been measured between certain solid-crystalline monolayers and fully liquidlike monolayers.[13] On the other hand, for hysteretic surfaces, the loading−unloading paths are time dependent, with the unloading path being above the loading path (implying $\gamma_R > \gamma_A$). In fitting the measured data of R, r, and L to eq 1, γ_A, γ_R, and K were obtained independently, where K is a purely mechanical elastic constant of the supporting material (including the mica sheets and glue) in each experiment.

Friction Measurements. Friction experiments were carried out using a new sliding attachment, the "bimorph slider".[14] The lower surface is supported at the end of a double-cantilever spring attached to the ends of two parallel piezoelectric bimorph strips. Normal forces are measured by the double-cantilever spring and lateral movement is accomplished by applying a dc or ac voltage across the bimorph strips. For low applied voltages (less than 100 V) the lateral displacement of the lower surface is proportional to V. The maximum applied displacement in a typical experiment was about 100 μm. In the friction experiments, a triangular voltage signal was applied to the bimorph slider to make the lower surface move at a constant velocity. The lower surface moves in one direction until the turning point and then in the reverse direction, repeatedly. The sliding velocity is controlled by changing the amplitude or frequency of the triangular voltage signal. In this study, sliding velocities ranged from 10 Å/s to 40 μm/s.

Friction forces are measured by means of a friction force-measuring attachment, or "friction device".[1,14] The upper surface is supported from a translation stage by four vertical friction springs with strain gauges. The four strain gauges make up the four arms of a Wheatstone bridge which is used to measure the lateral displacement produced on the upper surface by the motion of the lower surface (the bimorph slider). The friction device also has the capability of driving the stage supporting the upper surface at a constant velocity using a mechanical drive that is powdered by a variable speed dc motor with an encoder readout. When sliding is made in this way, one can generate movement and measure the resulting friction forces solely with the friction device. The bimorph slider only generates movement and so must be used in combination with the friction device to measure the friction forces as well. The friction device−bimorph slider combination is shown in a highly schematized way in Figure 1.

There are advantages to using the friction device and bimorph slider in the same experiment. If one moves the surfaces only with the friction device motor, the maximum displacement attainable is ∼5 mm. This allows one to measure large friction forces. However, the range of sliding velocities attainable with the friction device motor is limited to 3−4 decades—much less than the range of 7 decades attainable with the bimorph slider. In this study, we used the bimorph slider + friction device combination to measure *kinetic* friction forces because we could choose a wide range of sliding velocities. On the hand, we used the friction device motor to move the surfaces when we measured *static* friction forces because these forces (e.g., stiction spikes) were sometimes very high after a long stopping time.

Materials and Surface Preparation via Langmuir−Blodgett (LB) Deposition. The material under investigation is a double-chained cationic fluorocarbon surfactant, TAFC (*N*-(α-(trimethylammonio)acetyl)-*O*,*O*′-bis(1*H*,1*H*,2*H*,2*H*-perfluorodecyl)-L-glutamate chloride, $(C_8F_{17}\text{-}C_2H_4)_2$-L-Glu-Ac-$N^+$-$(CH_3)_3Cl^-$), obtained from Sogo Pharmaceuticals, Ltd, Japan, and used as received. Depositions were carried out in an all-Teflon LB trough (surface area 575 cm^2) filled with deionized Millipore-Q^+ purified water as the subphase.[15] The deposition temperature was held constant at 23 °C. The surface pressure was measured with a Wilhelmy-type surface balance.

The TAFC surfactant was dissolved in a chloroform:methanol mixture (95:5 by volume) to a total concentration of 1 mg/mL. Before the solution was spread on water, two bare mica sheets already mounted on cylindrical silica disks were immersed into the subphase quickly. After spreading the surfactant solution on the water surface, 20 min was allowed for solvent evaporation. The monolayer was then compressed to a surface pressure of 30 mN/m or 15 mN/m, corresponding to molecular areas of 50 Å^2 and 60 Å^2, respectively (the molecular areas were obtained from a pressure−area isotherm measurement). Since the maximum packing density of a fluorocarbon chain is about 25 Å^2, a molecular area of 50 Å^2 corresponds to an almost close-packed monolayer for this double-chained surfactant.[16] The mica surfaces were subsequently withdrawn from the solution at a speed of 4 mm/min while maintaining a constant surface pressure.

Experimental Procedure. After the deposition, the two mica-mounted disks were installed into the SFA. The SFA chamber was then purged with dry nitrogen gas for 12 h, and P_2O_5 was placed inside the chamber to ensure the desired atmospheric condition of 0% relative humidity. The whole experimental room was kept at a fixed temperature (to ±0.1 °C) for experiments in the range 15−35 °C; for experiments at 42 °C the SFA3 bathing chamber was heated by two resistive heating rods that were inserted into the steel walls of the chamber.

Results

Typical Friction Traces. First we show some typical friction traces obtained in this study. Figure 2b shows a characteristic (real) friction trace obtained using a combination of the bimorph slider and friction device when a triangular voltage is applied to the bimorph slider (Figure 2a), that is, when the lower surface

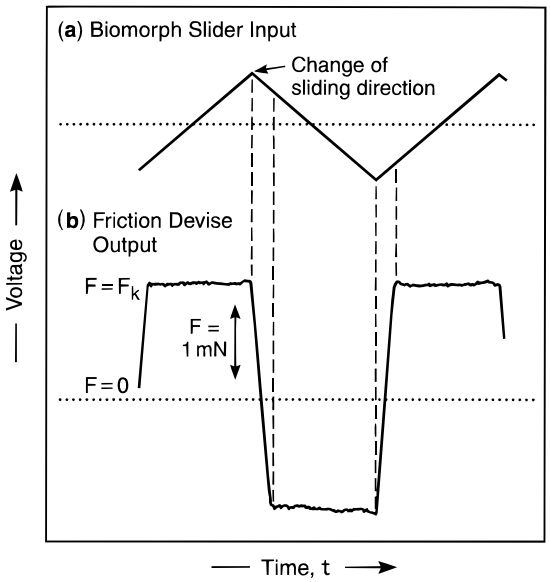

Figure 2. Typical fraction trace (friction force−time plot) obtained in this study. The sample is a fluorocarbon monolayer of TAFC of molecular area $a = 50$ Å^2. (a) Applied voltage to the driver (bimorph slider). (b) Output voltage of friction device (proportional to the vertical friction force scale as shown). Sliding conditions: sliding velocity $V = 0.42$ μm/s, temperature $T = 25$ °C, applied load $L = 15$ mN.

moves horizontally at a constant sliding velocity. In the beginning the upper surface, supported by the friction device, moves together with the lower surface. When the lateral force at the interface reaches the friction force ($F = F_k$) the surfaces begin to slide and the friction device strain gauge outputs a constant voltage (Figure 2b). Figure 2 shows a typical example of "smooth sliding" friction. This type of friction, in which the static and kinetic friction forces were the same, $F_s = F_k$, was obtained in most of our experiments. When the moving direction of the bimorph is reversed, sliding stops momentarily as the two stuck surfaces move together in the opposite direction until the critical friction force is again attained and sliding is resumed.

If the stopping time is long, or if the sliding velocity is below a certain critical velocity, the monolayers on the surfaces relax and freeze (nucleate then solidify or become amorphous) during stopping or on changing the sliding direction.[2] When sliding resumes, the initial friction force (F_s) is higher than the kinetic friction force (F_k) because melting of the monolayer is now needed to restart sliding. When this happens, "stiction spikes" are obtained on the friction traces (Figure 3). In this study, stiction spikes were obtained when the sliding velocity was lower than 0.05 μm/s (500 Å/s). The stiction spike height ($\Delta F = F_s - F_k$) increases with the stopping time and is also related to the stick−slip amplitude. These relations were analyzed in the different experiments (described below).

Figure 4 shows the various kinetic friction trace patterns obtained in this study. It is known that stick−slip often disappears abruptly at some critical velocity, V_c,[4,6] and this was found to be the case here: if the sliding velocity was higher than V_c, the sliding pattern changed abruptly from stick−slip to smooth sliding. For fluorocarbon monolayers of TAFC, V_c was generally below 10 Å/s, so that smooth sliding—illustrated by the friction trace of Figure 4a—was observed in most of our experiments. When sliding velocities lower than V_c were chosen, stick−slip type sliding appeared (Figure 4b) whose frequency decreased and whose amplitude ΔF increased with decreasing sliding velocity (Figure 4c).

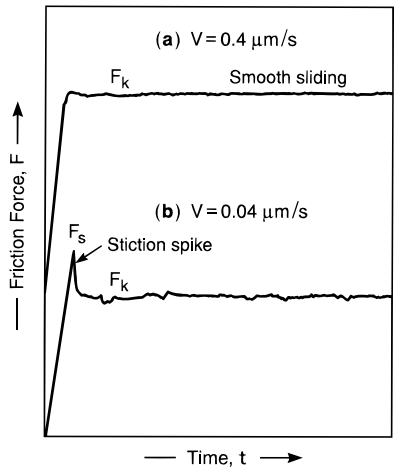

Figure 3. Stiction spike prior to steady kinetic sliding. Stiction spikes were observed for sliding velocities lower than 0.05 μm/s. Sliding conditions: $a = 50$ Å^2, $T = 25$ °C, $L = 25$ mN. Note that the time scales for (a) and (b) are not the same.

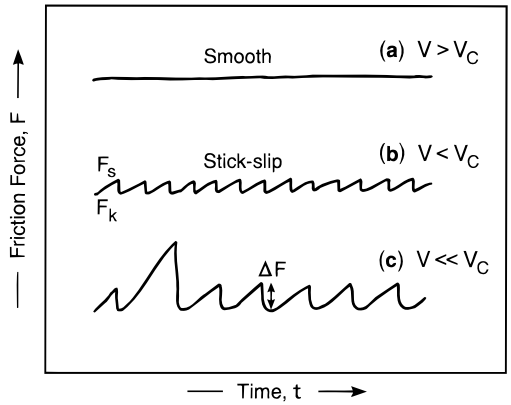

Figure 4. Exact reproductions of friction traces obtained at the same load and temperature but different sliding velocities. Stick−slip appears below some critical sliding velocity, V_c. Typical V_c values for fluorocarbon monolayers of TAFC were of order 10 Å/s (0.001 μm/s). The stick−slip amplitude ($\Delta F = F_s - F_k$) increases with deceasing sliding velocity below V_c. In the example shown here, $V_c \approx 8$ Å/s, (a) $V = 10$ Å/s, (b) $V = 6$ Å/s, (c) $V = 3$ Å/s.

Figure 5 shows the friction traces obtained after stopping and restarting. In these measurements, the lower surface was fixed and the upper surface was moved by the friction device motor. As mentioned previously, the stiction spike height ΔF increases with the stopping time, t. When sliding is stopped, some molecular relaxation occurs and the friction force initially decreases slightly. If the stopping time was shorter than a certain well-defined time (the characteristic nucleation time, τ_0) there was no measurable stiction spike ($\Delta F = 0$), and when sliding was resumed it proceeded as if the surfaces had never been at rest (Figure 5a). However, when the stopping time was longer than τ_0, a high stiction spike was observed when sliding was resumed (Figure 5b). The spike height increased with stopping time (Figure 5c). In this experiment $\tau_0 = 12$ s, but τ_0 was dependent on the temperature, applied load, and sliding velocity.

Effects of Sliding Velocity and Load on Kinetic Friction. In what follows, we show some results of our friction experiments on fluorocarbon monolayers of TAFC having molecular areas of 50 and 60 Å^2, at temperatures 15, 25, 35, and 42 °C, and zero relative humidity. From an industrial point of view it is also important to know the friction in humid conditions.[17] However, we soon found that fluorocarbon monolayers of TAFC were easily damaged during sliding in the presence of water

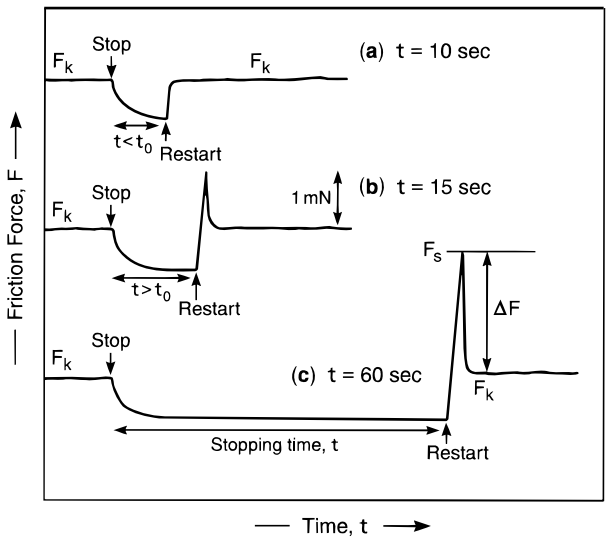

Figure 5. Stiction spike measurements. Sliding is stopped for a certain time, *t*, then restarted; meanwhile the friction force *F* is continually measured as a function of time. If the stopping time is shorter than the characteristic "nucleation time" τ_0, there is no change in the friction when it is restarted. However, when the stopping time exceeds τ_0, a stiction spike appears that whose height ΔF increases with the stopping time. In this experimental, $T = 25$ °C, $L = 10$ mN, $V = 0.7$ μm/s, $\tau_0 \approx 12$ s.

vapor, even when the applied load was zero (i.e., in self-adhesive contact). This damage was caused by the following mechanism: [15] water molecules in humid air penetrate into monolayers and form a hydration layer at the surfactant headgroup/mica interface. This hydration layer lifts the monolayer off the mica surface and thereby decreases the adhesion strength of the interface. When sliding begins, the molecules in the monolayers come off easily from the mica substrates and form small wear particles; this is damage. For this reason, all our experiments were carried out under 0% relative humidity, i.e., with totally dry surfaces.

Figure 6 shows typical friction forces (a) and shear stresses (b) versus sliding velocity at different loads. All the friction forces increased monotonically with sliding velocity (Figure 6a), which is typical of "liquidlike" sliding.[3] The friction forces also increased with applied load except for a decrease between 20 and 30 mN (see Figure 7a). The shear stresses also increased with sliding velocity (Figure 6b), but the load dependence was more complicated (Figure 7b). All curves in Figure 6 were obtained at 15 °C; results at other temperatures showed the same trends in their dependence on sliding velocity.

Figure 7 shows the same friction forces (a) and shear stresses (b) versus load at different sliding velocities. We may note the finite friction forces observed at zero loads due to the finite adhesion of the surfaces. The shear stresses (Figure 7b) were almost constant at fixed sliding velocities except for a kink at $L \approx 20$ mN. The shear stresses also increased with sliding velocity and displayed similar trends to the friction forces. Similarly complex load-dependent friction traces were measured at 25 °C, and are discussed below.

Effects of Temperature on Kinetic Friction. Figure 8 shows the effects of temperature on the shear stresses *S* versus sliding velocity *V* at two different applied loads *L* and pressures *P*. The shear stresses exhibited a minimum at $T \approx 30$ °C and a shallow minimum at $V \approx 10^{-2}$–10^{-3} μm/s at high loads.

Figure 9 shows the effect of temperature on the friction forces (a) and shear stresses (b) versus applied load or pressure (c) at constant sliding velocity ($V = 4.2$ μm/s). Changing the sliding

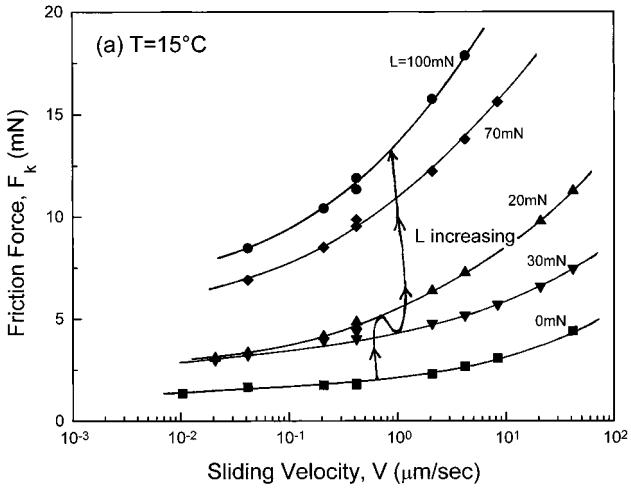

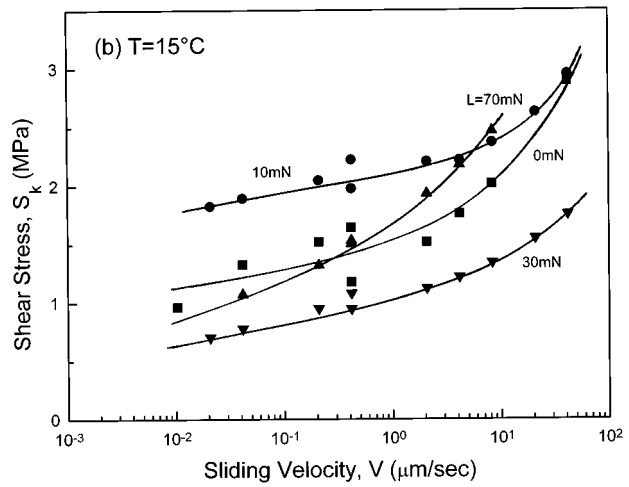

Figure 6. (a) Kinetic friction forces as a function of sliding velocity of fluorocarbon monolayers of TAFC at $T = 15$ °C. The molecular area was $a = 50$ Å^2. (b) The same data plotted as shear stress (S = friction force/contact area = F/A) against sliding velocity, *V*.

velocity didn't change the shapes of these curves much (data not shown). The data points were obtained from four different contact positions or samples, having different radii, contact areas, and elastic moduli. The applied pressure was taken as the abscissa in Figure 9c to normalize the load effects. The limited range of the measurements at 35 and 42 °C is due to the occurrence of irreversible surface damage above a certain load. This damage probably occurred because of the buckling of the close-packed monolayers caused by the stresses induced by the temperature changes. The effects of load on the shear stresses at different temperatures were complex: The friction forces and shear stresses were largest at 15 °C, decreased with increasing temperature, reached a minimum at around 25−35 °C, and increased again above 35 °C. However, the finer details of the underlying trends were difficult to uncover. Significantly, the shear stresses appeared to plateau at high loads or pressures.

Stiction Spike Measurements. We now turn our attention to the stiction spikes. The relation between the stiction spike heights and surface stopping times for various applied loads, temperatures, and sliding velocities were studied. The results are shown in Figures 10−12. Stiction spike heights normalized by the contact area are plotted as the ordinates and stopping times as the abscissae. The shapes of the curves consist of three parts. First, there is no stiction ($\Delta F = 0$) when the stopping time is less than the characteristic "nucleation" time, τ_0, as previously described.[4] Second, when the stopping time exceeds

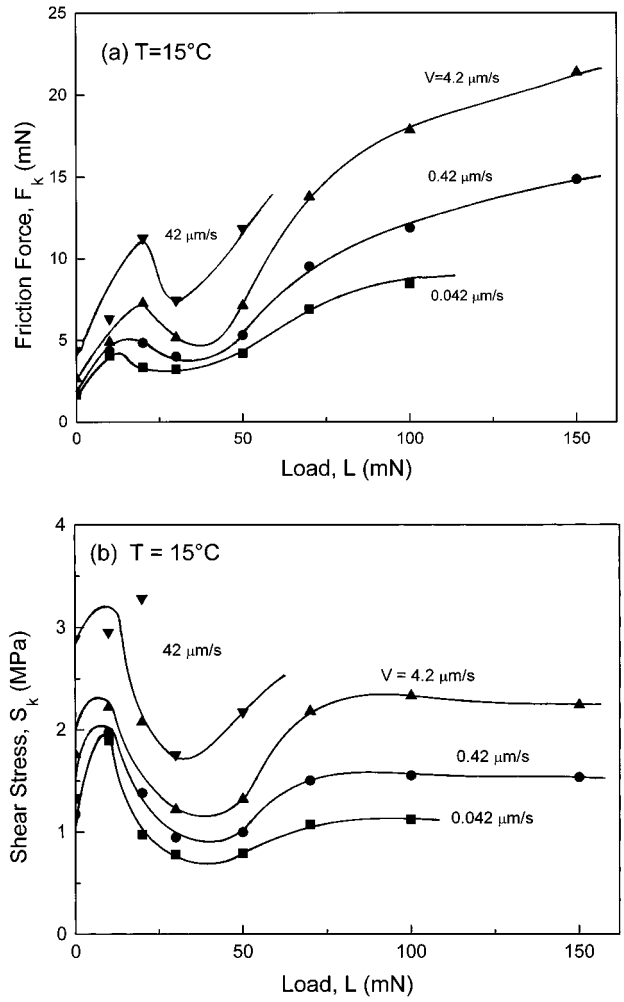

Figure 7. Kinetic friction forces (a) and shear stresses (b) as a function of applied load. Data corresponds to the results of Figure 6. When fitted to eq 3, we obtain $F_0 \approx 2-5$ mN and $\mu \approx 0.05-0.15$.

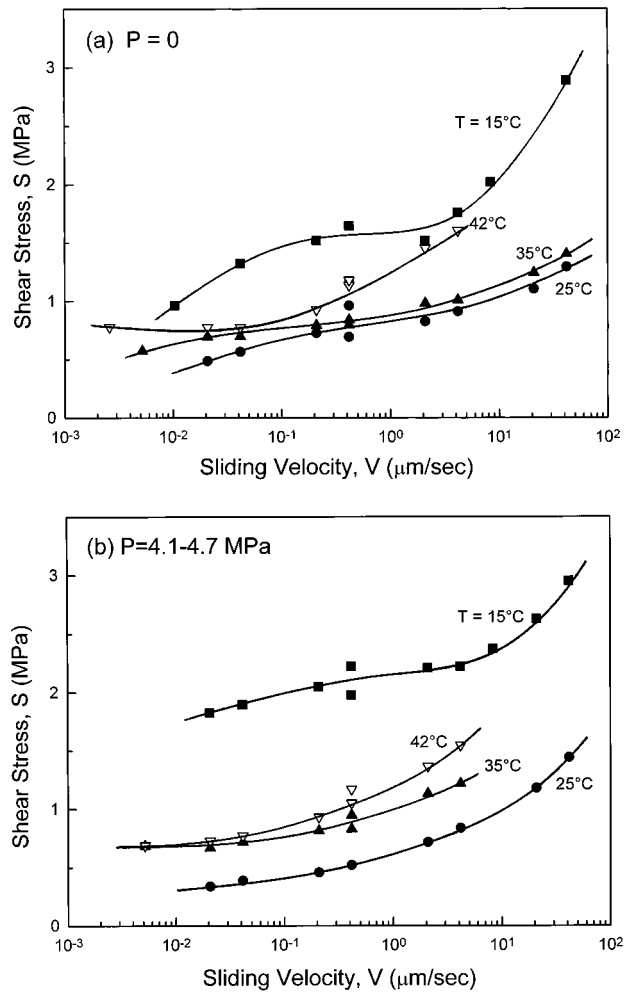

Figure 8. Kinetic shear stresses as a function of sliding velocity at different temperatures. The molecular area was 50 Å^2 for three curves and 60 Å^2 for the fourth curve (at 42 °C). (a) Applied load, $L = 0$; applied pressure, P = load/area = $L/A = 0$. (b) $P = 4.7$ MPa at 15 °C, 4.2−4.4 MPa at 25 °C, 4.1 MPa at 35 °C, and 4.6 MPa at 42 °C ($a = 60$ Å^2). While the same applied pressure is recommended for comparisons, it is difficult to keep both L and P the same at different experiments, temperatures, and contact positions.

τ_0, a stiction spike appears whose height ΔF increases sharply and almost linearly with t. Third, the slope of the line decreases above a certain stopping time. In Figure 12 we find yet a fourth part, another bending point, where the spike height appears to reach a constant value (this saturation effect was also seen in ref 4). The trends recorded in Figures 10−12 may be summarized as follows: (i) Spike heights ΔF increase with decreasing load L, increasing temperature T, and increasing sliding velocity. (ii) Larger spike heights ΔF are associated with shorter characteristic stopping times, τ_0. The implications of these trends are discussed later.

Adhesion Hysteresis Measurements. When two surfaces approach in air, they jump spontaneously into adhesive contact as soon as the force gradient exceeds the spring constant of the supporting spring. Because of the adhesion, the initially curved surfaces deform to a flat contact (see Figure 1). The relation between contact radius and applied load was analyzed by the JKR equation (1), where the adhesion energy γ and elastic modulus K of the material were calculated by fitting the JKR equation to the experimental data points. Figure 13 shows a typical contact radius (r^3) versus load (L) curve for a loading/unloading cycle of two fluorocarbon monolayers of TAFC (molecular area, $a = 50$ Å^2) at 15 °C. The fit to eq 1 yields $\gamma_A = 7$ mJ/m^2 for the loading (advancing) branch and $\gamma_R = 28$ mJ/m^2 for the unloading (receding) branch. We note that the magnitude of the advancing energy, $\gamma_A = 7$ mJ/m^2, but not the receding energy, is equal to the equilibrium value for fluorocarbon surfaces composed of $-CF_3$ groups (Table 1). This effect has been observed before with hydrocarbon surfaces[3,15] where γ_A, but not γ_R, coincides with literature values for γ.

The difference between γ_A and γ_R in Figure 13 defines the adhesion energy hysteresis per unit area as $\Delta\gamma = (\gamma_R - \gamma_A) = 21$ mJ/m^2. Similar measurements were carried out at different temperatures and different molecular areas. The results are listed in Table 1. For molecular areas of $a = 50$ Å^2, increasing the temperature resulted in a decreasing γ_R and $\Delta\gamma$, presumably due to the increasing thermal motion of the molecules in the monolayers.

It may be noted that γ_A is not very different at the different coverages and temperatures, and always close to the equilibrium value of $\gamma = 6$ mJ/m^2 for close-packed $-CF_3$ groups. The higher value at $a = 60$ Å^2 may be partly related to the higher concentration of $-CF_2$ groups at the surface. We may note, too, that the magnitude of the hysteresis, $\Delta\gamma = (\gamma_R - \gamma_A)$, was determined mainly by the magnitude of γ_R. The trends in the adhesion hysteresis as a function of temperature and coverage, displayed in Table 1, are similar to those exhibited by the friction forces and shear stresses, described previously. These correlations are discussed further below.

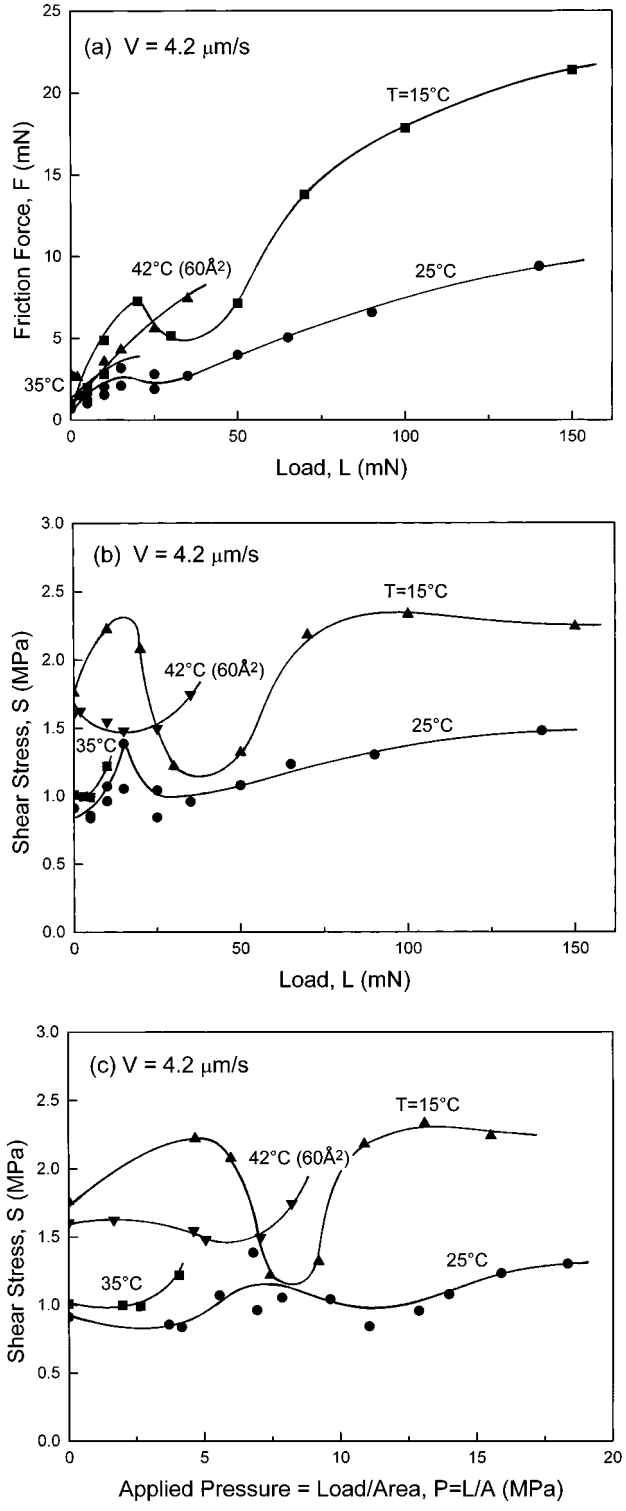

Figure 9. Kinetic friction forces (a) and shear stresses (b) as a function of applied load and pressure (c) at different temperatures. The molecular area was 50 Å^2 at 15−35 °C, and 60 Å^2 at 42 °C; the sliding velocity was $V = 4.2$ μm/s.

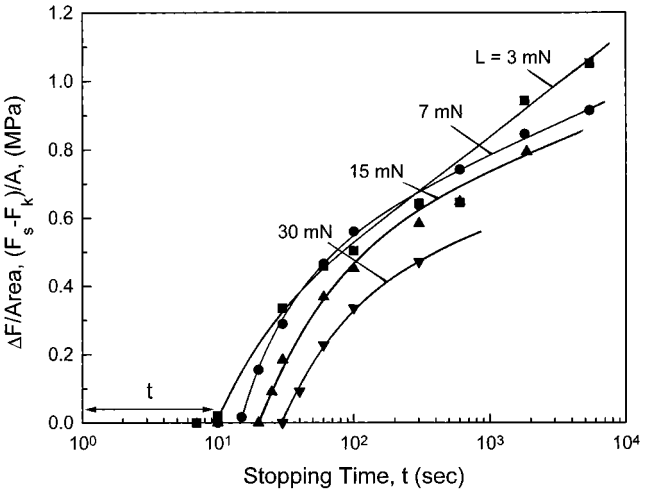

Figure 10. Effect of load L on stiction height ΔF (normalized by the contact area A) measured after different stopping times, t, for fluorocarbon monolayers of TAFC. $a = 50$ Å^2, $T = 25$ °C, $V = 0.33$ μm/s.

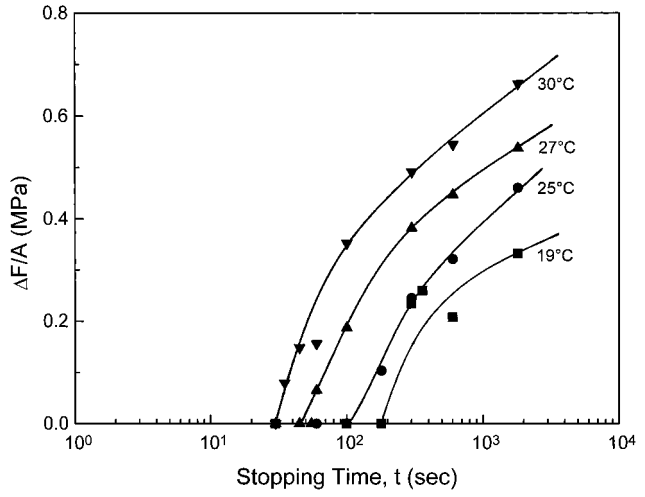

Figure 11. Effect of temperature T on normalized stiction spike height $\Delta F/A$. $a = 50$ Å^2, $L = 10$ mN, $V = 0.33$ μm/s.

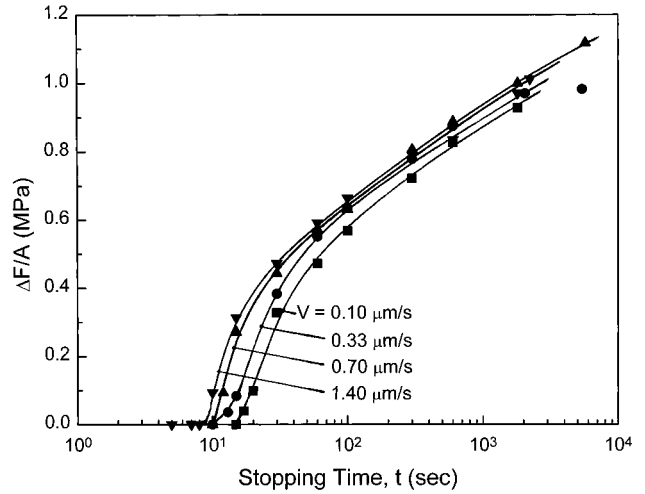

Figure 12. Effect of sliding velocity V on normalized stiction spike height $\Delta F/A$. $a = 50$ Å^2, $T = 25$ °C, $L = 10$ mN.

Discussion

"Friction Phase Diagram" Representation of Energy Dissipation. Energy dissipation processes at moving surfaces, such as friction and adhesion hysteresis, are determined by the molecular relaxations at the interface.[19] These relaxation processes include molecular collisions or vibrations, rotations, and cooperative rearrangements involving molecular clusters or 2D domains. Each of these processes has a characteristic relaxation time τ_0 and distance δ. For a simple liquid, these correspond to the time between molecular collisions and the molecular size, respectively. Cooperative relaxations usually have longer times and larger characteristic distances. During frictional sliding, when the characteristic "transit" time or "observation" time τ_t equals the relaxation time τ_0, energy

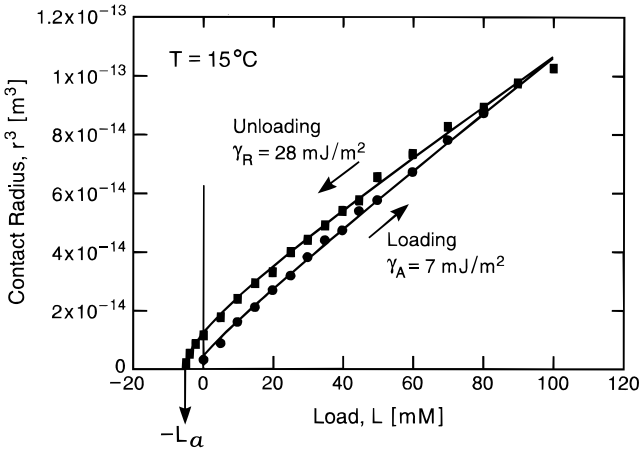

Figure 13. Contact radius versus load (r^3 vs L) curves for loading and unloading of two fluorocarbon monolayers. The fits, according to eq 1, yield for the loading branch $\gamma_A = 7$ mJ/m^2, unloading branch $\gamma_R = 28$ mJ/m^2, so that $\Delta\gamma = 21$ mJ/m^2 and $\gamma_m = 17.5$ mJ/m^2. The molecular area was $a = 50$ Å^2, $T = 15$ °C. The time needed to measure a complete loading/unloading cycle was about 20 min. L_a is the adhesion or "pull-off" force.

TABLE 1: Measured Surface Energies γ_A and γ_R (Units: mJ/m^2) Based on the JKR Equation, Eq 1[a]

	$a = 50$ Å^2		$a = 60$ Å^2	
	15 °C	25 °C	35 °C	$a = 60$ Å^2
advancing: γ_A	7	9	9	15
receding: γ_R	28	28	19	34
hysteresis: $\Delta\gamma = (\gamma_R - \gamma_A)$	21	19	10	19

[a] The literature value for the equilibrium surface energy of a perfluorolauric acid monolayer composed of close-packed $-CF_3$ groups is $\gamma = 6$ mJ/m^2. The value for PTFE whose surface is predominately $-CF_2$ groups is $\gamma = 18.5$ mJ/m^2. These values are determined from contact angle measures (ref 33, p 427]. Note that the advancing surface energies γ_A, i.e., those measured on loading but not on unloading, for the close-packed monolayers ($a = 50$ Å^2) are close to the equilibrium values. A similar effect was previously noted with hydrocarbon monolayers.[3,26]

dissipation (i.e., the kinetic friction force) is a maximum.[19] The ratio between τ_t and τ_0 is commonly known as the Deborah number, De, defined by

$$\text{De} = \text{relaxation time/transit time} = \tau_0/\tau_t \qquad (2)$$

so that maximum friction occurs when De ≈ 1. Thus, for a liquid or "liquidlike" film we expect the friction force to increase with the sliding velocity (as for a Newtonian liquid) until the sliding velocity $V = \delta/\tau_t$ reaches δ/τ_0, i.e., until $\tau_t = \tau_0$ (De = 1), above which velocity the friction force falls. Likewise, the adhesion hysteresis is a maximum when the loading−unloading time coincides with the characteristic relaxation time for (bulk) surface deformations or molecular interdiffusion across the interface.[3]

This approach to analyzing the friction and adhesion hysteresis of boundary lubricant films such as hydrocarbon surfactant monolayers is now well established, and energy dissipation versus sliding velocity (or shear rate) curves are often referred to as "friction phase diagrams".[20] Depending on the number of relaxation processes, these curves can display one or more maxima, separated by broad, shallow minima. The maxima can be separated by many decades (orders of magnitude) in sliding velocity or inverse transit time, since these generally have a log dependence on the dissipation energy. In this study, even though a large range (>4 decades) of sliding velocity were covered, the maxima in the friction forces were not always attained at all the temperatures studied, these being presumably located at higher or lower sliding velocities. However, a sufficiently clear picture emerges that shows that fluorocarbon monolayers participate in at least two different relaxation processes where—over the same range of temperatures, sliding velocities, and loads—hydrocarbon monolayers have only one.

Effects of Sliding Velocity and Temperature on Kinetic Friction. Over the range of velocities and temperatures studied, the friction forces F and shear stresses S generally increase with sliding velocity V (Figures 6 and 8), but a minimum occurs at $T \approx 30$ °C and $V \approx 10^{-2}$−10^{-3} μm/s, suggestive of two relaxation mechanisms. The trends also appear to be consistent with the time−temperature superposition principle where increasing T at constant V is equivalent to decreasing V at constant T.[21] Likewise, increasing the load shifts the $F(V)$ and $S(V)$ curves to *lower* sliding velocities (Figure 8), again as expected from the time−temperature superposition principle where increasing L at constant V is equivalent to decreasing V at constant T.[21]

However, the anticipated maxima in F at high and low T and V were not directly attainable in these experiments due to the lack of range. On the other hand, since stick−slip sliding was observed at very low sliding velocities (Figure 4), this indicates that below some very low velocity the friction force must again increase, i.e., that $F/dV < 0$ at $V < V_c$.[4,6] This is also consistent with the stiction spikes observed at low sliding velocities (Figure 3). These trends indicate that a "solid-like" high-friction region exists over some very low sliding velocity range ($V < 10$ Å/s) that is outside the range covered by these experiments. Additionally, the increasingly positive slope in the $F(V)$ curves with decreasing T (Figure 8) suggest that there is yet another maximum at some high velocity and, therefore, that another maximum exists at high V. The results of Figures 6−8 thus lead to the conclusion that there are (at least) two friction maxima, associated with two different molecular relaxation processes, in the friction phase diagram for fluorocarbon monolayers of TAFC. This is shown schematically in Figure 14a.

The same friction phase diagram can also be plotted as a function of temperature, as illustrated in Figure 14b, which is qualitatively consistent with the velocity phase diagram of Figure 14a via time−temperature superposition. The TAFC monolayers exhibit a minimum at around 30 °C (depending on the velocity) and, presumably, two maxima at $T < 15$ °C and $T > 42$ °C, which are discussed again below.

Effects of Load on Kinetic Friction. According to simple theories of friction, F is proportional to L, as given by

$$F = F_0 + \mu L \qquad (3)$$

where F_0 and μ are constants, defined as the zero-load friction and the coefficient of friction, respectively. This friction law has a broad range of applicability and is still the principal means of quantitatively describing the friction between surfaces. However, recent work on molecularly smooth surfaces has demonstrated that the friction force is not always proportional to the load (i.e., that μ is not independent of L), and that both F_0 and μ depend on the sliding velocity and temperature, especially when measured over a large range of V and T. For molecular smooth surfaces, strong adhesion is often observed at the interface and a finite friction force is detected even at zero load, defined by F_0, which has been found to be proportional to the real (molecular) contact area, A.[1,22−24] In this case, dividing through by A, eq 3 may be rewritten in the form

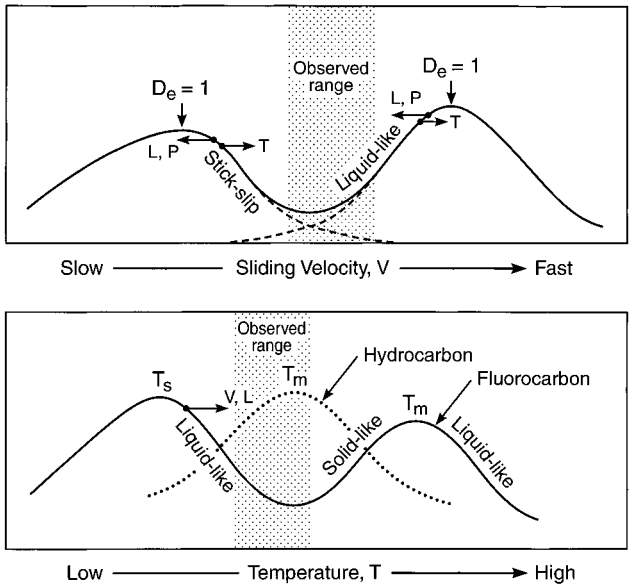

Figure 14. Schematic "friction phase diagrams" showing the effects of sliding velocity, load, and temperature on frictional energy dissipation (the friction force or shear stress). Similar plots can be constructed for adhesion energy hysteresis. The regions of the "phase diagrams" investigated in this study are represented by the shaded areas. Horizontal arrow indicate the directions which the curves are shifted to on increasing *T*, *L*, or *V*. Note that these directions can have a vertical components as well and that they may have different magnitudes for the different curves.

$$S = F/A = S_0 + \mu P \tag{4}$$

where S is the shear stress ($S = F/A$), S_0 is the critical shear stress ($S_0 = F_0/A$), and P is the applied pressure ($P = L/A$). Under "ideal" conditions, S_0 and μ are constants and L and A are related by the JKR equation (1). When S_0 dominates the friction force, we have "adhesion-controlled" friction, whereas when μ dominates, we have "load-controlled" friction.

Applying these equations to the experimental results, we see that the fluorocarbon monolayers have finite friction at zero load (Figures 7a and 9a) and, at higher loads, the shear stress S is almost constant (Figure 9b), viz. the friction force is proportional to the contact area. This implies that the friction is mainly "adhesion controlled", which is the same as previously seen with hydrocarbon surfactant monolayers at low loads or pressures.[1,22,24] (A transition to load-controlled friction is expected at much higher loads or pressures.[23])

Molecular Rearrangements during Sliding. An effect that has not been seen with hydrocarbon films was observed at low loads and temperatures, namely, the abrupt dip in both F and S at some critical load or pressure, independent of the sliding velocity (Figure 9). This is suggestive of a change in the molecular ordering or configuration at $P = 5-10$ MPa, which may be similar to the abrupt *velocity*-induced reduction in the kinetic friction force of certain hydrocarbon surfactant systems above some critical velocity, which was termed "superkinetic friction".[25] In those studies, the surfactant molecules were also anchored or physisorbed at one end to the surfaces, but were not close packed. The abrupt reduction in the friction was attributed to a shear-induced "combing" of the loosely-packed hydrocarbon chains into a more ordered, less interdigitated, and therefore lower-friction configuration.

In contrast, the load-induced friction reduction of the fluorocarbon surfactant is probably due to a different mechanism: fluorocarbon chains are relatively more bulky and rigid and do not interdigitate into each other (fluorocarbon surfactants do not form spherical micelles). Further, the molecules in these monolayers were almost close-packed, again eliminating any possibility of interdigitation. The friction between fluorocarbon monolayers is therefore not governed by the interdigitation of flexible, mobile chains across the interface but by the topography or "bumpiness" of the surfaces at the molecular level. Figure 15 shows the likely surface configuration and the proposed mechanism of load-induced "superkinetic friction" of fluorocarbon monolayers. The surface $-CF_3$ groups may be considered as bulky balls on a quasi-rigid surface lattice that fits into the opposite lattice when at rest. When a shear force is applied, the interface first dilates before sliding begins at a high kinetic friction force, as expected from the Cobblestone or Coulomb models of friction.[26] These high friction forces can be reduced by a change in the configuration of the molecules at the interface. In the case of hydrocarbon chains, this can be achieved by combining the chains to reduce their interdigitation. In the case of fluorocarbon molecules, this appears to be achieved by a different mechanism, namely, a smoothing out (flattening) of the surface molecular corrugations. For the TAFC monolayers studied here, other possible changes in molecular configuration at the interface may arise from one or more of the following molecular mechanisms: a change in the rotational angle of the three−F atoms at the surface, alignment of the axes of the double-chained molecules along the sliding direction, bending of the fluorocarbon chains near the tip of molecules, a

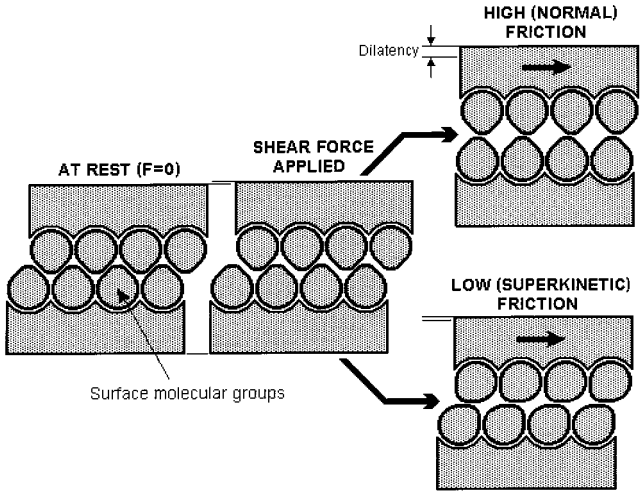

Figure 15. Proposed schematic model of the interfacial sliding of fluorocarbon surfactant monolayers. The bulky $-CF_3$ terminated chains are shown as modified semirigid balls that bite into each other when at rest. When a shear force are applied, sliding starts at the interface as an elastic displacement accompanied by interface swelling (dilatency) which continues until the yield point is reached ($F = F_S$) at which point kinetic sliding proceeds ($F = F_k$) as described by the Coulomb and Cobblestone models.[26] The surface is relatively bumpy and the friction force is consequently high. However, if an alternative route is possible—especially one that involves a lower force barrier to motion, this will become the preferred path. One such example is shown here where the molecular groups at the surfaces rearrange slightly to expose a smoother surface which in turn presents a reduced force barrier for sliding. This mechanism is proposed to account for the abrupt load-induced *reduction* in friction observed here with the TAFC monolayers over a certain range of loads. Other molecular rearrangements, involving large deformable clusters with few molecularly smooth contacts, may be responsible for the low friction of Teflon (PTFE) surfaces, as discussed in the text. These mechanisms are quite different from those occurring between hydrocarbon monolayers where chain interdigitation (rather than molecular reorientations) is believed to be the dominant mechanism giving rise to frictional energy dissipation and adhesion energy hysteresis at ambient temperatures.

TABLE 2: Comparison of Some Adhesion and Friction Properties of Hydrocarbon and Fluorocarbon Surfaces (All Values Are Approximate)

	hydrocarbon		fluorocarbon	
	close-packed monolayer ($a = 19$ Å^2)	amorphous surfaces (wax, polyethylene)	close-packed TAFC monolayer ($a = 25$ Å^2)	amorphous suface (Teflon)
literature values for γ (mJ/m^2)	24	25−32	6[a]	18.5[a]
friction forces	$S_0 = 0.1-4$ MPa[c]	$S_0 = 0$	$S_0 = 1-3$ MPa	$S_0 \approx 0$
$F = S_0A + \mu L$ ($T < T_m$)	$\mu = 0.01-0.10$[c]	$\mu = 0.20$[b]	$\mu = 0.05-0.15$	$\mu = 0.04-0.07$[b]
stiction and stick-slip spikes	large[c]		small	
critical temperatures as measured from friction force maxima	$T_c = 30-35$ °C (cf. $T_m \approx 30$ °C)		$T_1 < 15$ °C $T_2 > 42$ °C (cf. $T_m = 94$ °C)	

[a] Reference 33, p 427. [b] Reference 32, p 73. [c] References 3, 22, and 25.

change in the tilt angle of fluorocarbon chains. The driving force for these configuration changes is the high intrinsic friction force.

Such a surface geometry change at the molecular level is proposed as a general mechanism of friction reduction of rigid, bulky molecules. It is likely that the much lower friction of Teflon (PTFE) owes itself not to the low adhesion energy of these surfaces (more on this below) but to a special sliding/rolling configuration of the PTFE molecules between two shearing surfaces, which would be quite different from the situation where the molecules are held tightly in a rigid monolayer. This interpretation is consistent with previous reports of high friction of cross-linked fluorocarbon polymer surfaces which is significantly reduced on addition of free Teflon, even though the surface energy does not change.[35]

Stiction Spikes. As already mentioned, when sliding stops, the molecules at the interface rearrange from their kinetic (liquidlike or shear-ordered) sliding configuration back to their static (solidlike, frozen or amorphous) configuration. This processes takes a finite time, and involves a rapid nucleation step followed by a slower relaxation of the nucleated domains to the final frozen state.[4] On restarting the strain, the surfaces remain pinned until some yield point is reached. During this time the frozen configuration remains unchanged but deforms elastically up to the yield point when "melting" occurs; this is followed by a transition to kinetic sliding when the molecules revert to their kinetic sliding configurations.

The stiction spike height, ΔF, being the difference between the friction force at the yield point and during steady-state sliding, reflects the extent of the change in the molecular configurations between these two states. Stiction spikes do not appear when the stopping time is shorter than the characteristic nucleation time, τ_0. Spikes appear only for stopping times $t > \tau_0$ whose heights increase with t, presumably because the nucleated domains or configurations continue to grow laterally with time. From this molecular perspective, one would expect τ_0 and ΔF to be strongly affected by the mobility of the molecules trapped at the interface and to be correlated with each other. The effects of load and temperature on the spike heights—shown in Figures 10 and 11—reflect these trends: Increasing L or decreasing T both act to *decrease* the mobility of molecules so that it takes them longer to nucleate, resulting in a higher τ_0 and/or lower ΔF, as observed. The sliding velocity is also expected to affect the molecular configuration during shear,[4] and Figure 12 shows that τ_0 decreases while ΔF increases with increasing V. This suggests that the molecules become more shear-ordered at higher V, which could make it easier for them to freeze on stopping.

Correlation between Adhesion and Friction. Previous experiments on hydrocarbon surfaces have shown that friction and adhesion are not generally related when one compares the absolute magnitude of the friction force with the equilibrium adhesion force or energy.[3,18] However, friction and adhesion energy *hysteresis* are often well-correlated, as might be expected, since both are nonequilibrium, energy-dissipating processes. The adhesion energy hysteresis per unit area obtained in this study depended on the temperature and exhibited a minimum at around 35 °C as shown in Table 1. This trend is similar to the temperature dependence of the friction force, as shown in Figure 9, indicating that a correlation between friction and adhesion hysteresis also exists for fluorocarbon monolayers even though the molecular relaxation mechanisms may be different. This correlation may also be tested quantitatively using the simple equation that relates the friction force F or shear stress S to the adhesion energy hysteresis $\Delta\gamma$:[26]

$$S = F/A = 2\epsilon\Delta\gamma/\delta \tag{5}$$

where δ is a molecular dimension, A is the contact area, and ϵ ($\epsilon < 1$) is the fraction of energy transferred, as heat, per molecular collision during shear—the higher the transfer efficiency the higher will be the friction force. Inserting the measured value at 15 °C into the above equation: $\Delta\gamma = 21 \times 10^{-3}$ J/m^2 (Figure 13), and $\delta = 10^{-9}$ m, we obtain "theoretical" S values in the range $S = 4-40$ MPa for ϵ between 0.1 and 1.0. This may be compared with the experimental values for S at 15 °C of ~1−3 MPa (Figure 7). A more rigorous comparison would have to be done at similar rates or transit times, e.g., at sliding velocities = δ/loading−unloading time, which corresponds to slower sliding velocities where the experimental S is presumably higher.

Comparison with Hydrocarbon Surfaces. Table 2 compares the adhesion and friction properties of hydrocarbon and fluorocarbon surfaces, both monolayer and non-monolayer, using the data obtained here and from the literature. We distinguish between monolayer (ordered) surfaces and amorphous (disordered) surfaces since these have been found to give very different friction forces even when the adhesion energies are the same. We also distinguish between films or surfaces above and below the melting temperature T_m which, in monolayers and trapped interfacial films, may be different from the bulk values. The similarity and difference may be summarized as follows.

(1) *Adhesion*. It is well-known that the adhesion energy of fluorocarbon surfaces such as Teflon (PTFE) is lower than that of hydrocarbon surfaces. Typically, $\gamma_{HC} = 24-32$ mJ/m^2 compared to $\gamma_{FC} = 6-19$ mJ/m^2 (Table 1). These thermodynamic values are reflected in the JKR r^3-L plots as well as in the pull-off forces F_{ad} measured between such surfaces which are related to γ via the equation:[3,15]

$$F_{ad} = 3\pi R\gamma \quad (6)$$

Such measurements have yielded values for (equilibrium) surface energies of $\gamma_{HC} \approx 30$ mJ/m^2 for hydrocarbon surfaces in the solid, and liquid states[3,15,24,26] and, in this study, $\gamma_{FC} \approx 7-15$ mJ/m^2 for fluorocarbon monolayer surfaces (γ_A values in Table 1). Both of these sets of values are in good agreement with the thermodynamic values. One may note that the low value for the surface energy *per unit area* of $-CF_3$ groups is not due to the lower van der Waals force or pair potential between these groups but because of the larger area they occupy than $-CH_3$ groups (25 Å^2 compared to 19 Å^2).[30] The pair potential between two $-CF_3$ groups is actually larger than that between two $-CH_3$ groups,[31] a matter that also has relevance to their friction forces, discussed below.

(2) Friction Forces. Typical critical shear stresses S_0 (defined by eqs 3 and 4) for hydrocarbon monolayer surfaces have ranged from 0.1 to 5 MPa, and friction coefficients μ have ranged from 0.15 to below 0.001.[3] This large range covers monolayers in both the solid crystalline, amorphous, and fluid states, but also depends on the sliding velocity, humidity, and presence of organic vapors. For hydrocarbon monolayers in the frozen state only ($T < T_m$), which should be similar to the phase state of the fluorocarbon monolayers studied here, typical values have been $S_0 = 0.1-4$ MPa and $\mu = 0.01-0.10$, depending on the sliding velocity and relative humidity.[3,22,25] In comparison, the shear stresses and friction coefficients obtained for the fluorocarbon monolayers in this study are $S_0 = 1-3$ MPa (Figures 6−8) and $\mu = 0.05-0.15$ (Figure 7a). Both of these parameters cover a smaller range but are generally higher than those of hydrocarbon surfactants. The higher friction of fluorocarbon monolayers compared to hydrocarbon monolayers has been noted before in SFA measurements,[27] pin-on-disk measurements,[28] and AFM measurements.[29] These findings are surprising in view of the much lower adhesion energy of fluorocarbon surfaces, and they appear to be inconsistent with the low friction coefficient of Teflon (PTFE) surfaces: $\mu = 0.04-0.07$[32] when compared to $\mu = 0.05-0.15$ for the fluorocarbon monolayer surfaces obtained here.

The differences between hydrocarbon and fluorocarbon *monolayers* arise because the molecular mechanisms responsible for both adhesion and friction are different in the two systems: As already noted, the van der Waals pair potential for two $-CF_3$ groups (as opposed to the surface energy per unit area) is actually larger than that between two $-CH_3$ groups,[31] and there are arguments to suggest that the pair potential is more important in determining friction forces since thermal effects are less effective in reducing the activation force barrier to the shearing of larger, more rigid molecules, i.e., less effective in reducing ϵ in eq 5.[30] This is yet another way of saying that it is the adhesion *hysteresis*, rather than the *equilibrium* adhesion energy, which must be compared with the friction forces.

The differences between Teflon and fluorocarbon monolayer surfaces appear to be mainly due to the absence of the adhesion-controlled contribution in the case of Teflon surfaces in eqs 3 and 4 (note that the values for μ are not very different). It is highly unlikely that the friction of Teflon proceeds by the sliding of molecularly smooth layers across each other, and there is no evidence for this. More likely, clusters of PTFE molecules roll and deform as they squeeze past each other, so that the real contact area is small and the adhesion contribution to E is negligible. In contrast, the present study and those referred to above[27−29] apply only to the sliding of smooth undamaged monolayer-coated surfaces where a finite friction force exists already at zero load.

(3) Friction Phase Diagrams. The effects of sliding velocity, load, and temperature on the kinetic friction of fluorocarbon surfactants can be represented by similar "friction phase diagram" plots that obey the time−temperature superposition principle as those of hydrocarbon surfaces (Figure 14b). For fluorocarbon surface there appears to be at least two energy dissipation maxima that correspond to two different molecular relaxation mechanisms, one well below the other well above room temperature. We attribute these to solid−solid and melting transitions, respectively (Table 2). In contrast, hydrocarbon monolayers exhibit a maximum near room temperature, close to their bulk melting temperature.[3,34]

(4) Effect of Load (Superkinetic Sliding Transitions). Over a narrow velocity range an abrupt *reduction* in the friction force occurs with *increasing* load. A similar effect was previously observed with hydrocarbon monolayers,[25] but there the abrupt reduction was brought about by an increase in sliding velocity. The two mechanisms are probably different: with the hydrocarbon molecules, the interdigitated chains can become combed into a lower-friction dynamic configuration above some critical sliding velocity, whereas the fluorocarbon molecules, a lower-friction configuration may be brought about by rearranging the bulky surface $-CF_3$, as illustrated in Figure 15, which is achieved above some critical load or pressure, rather than velocity.

(5) Stick−Slip Sliding and Stiction. As for hydrocarbon monolayers, stick−slip friction was observed below some critical sliding velocity, V_c. However, with fluorocarbon monolayers V_c was very low, typically 1−10 Å/s (Figure 4), and not very dependent on the load and temperature. In contrast, V_c for hydrocarbon monolayers is generally higher and much more sensitive to the experimental conditions such as the load, temperature, relative humidity, and presence or condensing hydrocarbon vapors.[4] We should note, however, that these differences apply only to the range of temperatures (near room temperature), sliding velocities (10 Å/s to 50 μm/s), and pressures (up to 10 MPa) at which these comparisons have been made. But they nevertheless point to different molecular configurations and relaxations for hydrocarbon and fluorocarbon surfaces.

From a practical perspective, the low V_c and its insensitivity to experimental conditions offers a large advantage to fluorocarbon surfactants as lubricants. The friction is stable, and only smooth sliding is observed over a large range of conditions. This is particularly important in practice because surface damage during sliding often occurs because of stick−slip.

We now turn our attention to the related stiction spikes, which also cause damage when surfaces are sheared from rest. The stiction spike heights of the fluorocarbon surfactant were generally lower than with hydrocarbon surfactants,[25] probably due to the greater interdigitation that can occur with hydrocarbon chains. But the fluorocarbon spike height increased much longer with stopping time, i.e., took longer to plateau, than do hydrocarbon spikes.[4] It appears that the bulkier and more solidlike fluorocarbon groups have less ability to interdigitate than do hydrocarbon chains, but it also appears that they take longer to do that precisely because they are in a more solidlike state. The lower stiction spike heights of fluorocarbon surfaces is yet another beneficial property for good lubricity and preventing damage.

(6) Effect of Temperature. Temperature affects the mobility of the molecules in monolayers, and this changes the energy dissipation processes. For hydrocarbon monolayers, increasing the temperature near room temperature makes the films more

liquidlike (Figure 14). There is greater interdigitation across the interface, but it is also easy to disentangle the chains because of their high mobility; consequently the frictional energy dissipation is low and decreases with increasing T. At the low-temperature end, the chains freeze and do not interdigitate, so that again the friction is low. At some intermediate temperature, near T_m, when the chains are in the "amorphous state" between the liquidlike and solidlike states, there is maximum energy dissipation during sliding because rate of molecular interdigitation at the interface is high in relation to the slower disentanglement rate. Experimentally it has been found that these temperatures are close to the chain-melting temperatures of the chains[4,34] as illustrated in Figure 14. In the case of fluorocarbon monolayers, their high melting temperature (T_m = 94 °C for TAFC) shifts their peak friction to well above room temperature. On the other hand, our experiments suggest that another type of phase transition, probably one involving solid−solid reordering as illustrated in Figure 15, occurs at a temperature well below room temperature. The net result of this is that at room temperature the friction force is a minimum—lying between two well-separated maxima (Figure 14). This difference is yet another reason for the low friction coefficient of fluorocarbon compared to hydrocarbon monolayers, and it may also play a role in the low friction displayed by PTFE (Teflon) surfaces and coatings.

Conclusions

The following conclusions can be drawn from this study:

(i) The kinetic friction behavior of fluorocarbon *monolayers* of TAFC has both an adhesion component (friction force proportional to real contact area) and a load component (friction force proportional to applied load), and is mainly "adhesion controlled" at low loads. For smooth surfaces this implies a high friction force.

(ii) The friction dependence on sliding velocity and temperature can be represented by a "friction phase diagram" obeying the principle of time−temperature superposition, which has two energy dissipation maxima, one well above the other well below room temperature, as well as at high and low sliding velocities.

(iii) Adhesion hysteresis measurements for fluorocarbon monolayers show a direct correlation with the friction forces (shear stresses).

(iv) The adhesion energy (per unit area) of fluorocarbon monolayer surfaces is low, and similar to the low value for Teflon (PTFE) surfaces, but the friction forces are higher than for Teflon surfaces, because in monolayers the molecules are well-ordered and the surfaces remain molecularly smooth during sliding, while at Teflon surfaces they are in a highly disordered state and "rough" sliding prevails.

(v) Chain interdigitation, which is the most important molecular mechanism for friction and adhesion hysteresis of hydrocarbon surfaces (near room temperature) does not play a major role for fluorocarbons. Instead, the geometry of the bulky fluorocarbon groups at the surfaces and its change at the molecular and submolecular levels during shear is the most important mechanism for fluorocarbon friction. This mechanism is probably different in the case of Teflon (PTFE) surfaces where the fluorocarbon molecules are not anchored to a solid substrate.

(vi) Over a certain range of loads, increasing the load can decrease the friction force (load-induced "superkinetic friction"), probably caused by a pressure-induced change in the orientaton of the surface $-CF_3$ groups.

(vii) In spite of their higher intrinsic friction, fluorocarbon surfactant monolayers can act as good lubricant films because (a) their tribological performance is not very sensitive to temperature, sliding velocity, and load (hydrocarbon monolayers are much more sensitive to these factors[3]); (b) they exhibit smooth rather than stick−slip sliding over a wide range of sliding velocities; and (c) they have low stiction spikes, which are a major cause of surface damage.

Acknowledgment. We thank Alan Berman and You-Lung Chen for enlightening discussions and Robert Hill for his excellent technical assistance. S.Y. thanks Kao Corp. for their support.

References and Notes

(1) Homola, A. M.; Israelachvili, J. N.; Gee, M. L.; MuGuiggan, P. M. *J. Tribol.* **1989**, *111*, 675.
(2) Gee, M. L.; McGuiggan, P. M.; Israelachvili, J. N.; Homola, A. M. *J. Chem. Phys.* **1990**, *93*, 1895.
(3) Yoshizawa, H.; Chen, Y. L.; Israelachvili, J. *J. Phys. Chem.* **1993**, *97*, 4128; *Wear* **1993**, *168*, 161.
(4) Yoshizawa, H.; Israelachvili, J. *J. Phys. Chem.* **1993**, *97*, 11300.
(5) Granick, S. *Science* **1991**, *253*, 1374. Carson, G.; Hu, H.-W.; Granick, S. *Tribol. Trans.* **1992**, *35*, 405.
(6) Berman, A. D.; Ducker, W. A.; Israelachvili, J. N. *Langmuir* **1996**, *12*, 4559.
(7) Gitis, N. V.; Volpe, L.; Sonnenfeld, R. In *Long-Term Stiction at the Magnetic Thin Film Disk-Slider Interface*; Bhushan, B., Ed.; Advances in Information Storage Systems v. 3, ASME: New York, 1991.
(8) Nabata, Y.; Aoki, Y.; Yamada, S.; Maki, K. *Tribology and Mechanics of Magnetic Storage System*; 1994, Vol. 4, STLE Special Publication, SP-36, 1.
(9) Barlow, M.; Braitberg, L.; Dunn, V.; Frew, D. *IEEE Trans. On Mag.* **1987**, *23*, 33.
(10) Israelachvili, J. N.; McGuiggan, P. M. *J. Mater. Res.* **1990**, *5*, 2223.
(11) Israelachvili, J. N. *J. Coll. Inter. Sci.* **1973**, *44*, 259.
(12) Johnson, K. L.; Kendall, K.; Roberts, A. D. *Proc. R. Soc. London* **1971**, *A324*, 301.
(13) Chen, Y. L.; Helm, C. A.; Israelachvili, J. N. *J. Phys. Chem.* **1991**, *95*, 10736.
(14) Luengo, G.; Schmitt, F. J.; Hill, R.; Dhinojwala, A.; Israelachvili, J. N. *Macromolecules* **1997**, *30*, 2482.
(15) Chen, Y. L.; Israelachvili, J. N. *J. Phys. Chem.* **1992**, *96*, 7752.
(16) Takahara, A.; Morotomi, N.; Hiraoka, S.; Gigashi, N.; Kunitake, T.; Kajiyama, T. *Macromolecules* **1989**, *22*, 617.
(17) Bhushan, B. *Tribology and Mechanics of Magnetic Storage Devices*, Springer-Verlag: New York, 1990.
(18) Israelachvili, J. N.; Chen, Y. L.; Yoshizawa, H. *J. Adhesion Sci. Technol.* **1994**, *8*, 1231.
(19) Israelachvili, J.; Berman, A. *Isr. J. Chem.* **1995**, *35*, 85.
(20) Luengo, G.; Israelachvili, J.; Granick, S. *Wear* **1997**, *200*, 328.
(21) Ferry, J. D. *Viscoelastic Properties of Polymers*, 3rd ed.; Wiley: New York, 1980.
(22) Homola, A. M.; Israelachvili, J. N.; McGuiggan, P. M.; Gee, M. L. *Wear* **1990**, *136*, 65.
(23) Berman, A. D.; Israelachvili, J. N. In *Micro/Nanotribology and its Applications*; NATO Advanced Science Institute Series; Bhushnan, B., Ed.; Kluwer Academic Publishers: Dordrecht, 1997; pp 317−329. Also A. Berman and J. Israelachvili, Unpublished results.
(24) Israelachvili, J. N. In *Fundamentals of Friction*; Singer, I. L., Pollock, H. M., Eds.; Kluwer Academic Publishers: The Netherlands, 1992; pp 351.
(25) Yoshizawa, H.; McGuiggan, P.; Israelachvili, J. *Science* **1993**, *259*, 1305.
(26) Israelachvili, J. N. *CRC Handbook of Micro/Nanotribology*; CRC Press: Boca Raton, FL, 1995; Chapter 8, pp 267−319.
(27) Briscoe, B. J.; Evans, D. C. *Proc. R. Soc. London* **1982**, *A380*, 389. Briscoe, B. J.; Evans, D. C.; Tabor, D. *J. Colloid Interface Sci.* **1977**, *61*, 9.
(28) Chaudhury, M. K. *Mater. Sci. Eng.* **1996**, R16 (19) *3*, 97.
(29) Meyer et al. *Thin Solid Films* **1993**, *220*, 132.
(30) Luengo, G.; Campbell, S. E.; Srdanov, V. I.; Wudl, F.; Israelachvili, J. N. *Chem. Mater.* **1997**, *9*, 1166.
(31) *CRC Handbook of Solubility Parameters and Other Cohesion Parameters*; Barton, A. F. M., Ed.; CRC Press: Boca Raton, FL, 1983; pp 81.
(32) *Handbook on Friction, Lubrication and Wear Technology*; The Materials Information Society, ASM International: Materials Park, OH, 1992; Vol. 18.
(33) Reference 31, Table 1, p 427.
(34) Liu, Y.; Evans, D. F.; Song, Q.; Grainger, D. W. *Langmuir* **1996**, *12*, 1235.
(35) Hunston, D. L.; Griffith, J. R.; Bowers, R. C. *Ind. Eng. Chem. Prod. Res. Dev.* **1978**, *17*, 10−14.